Decay of the double–K-shell-vacancy state in silver atoms created in the decay of 109Cd

Horvat, V.; Ilakovac, Ksenofont

Decay of the double—K-shell-vacancy state in silver atoms created in the decay of ^{109}Cd

V. Horvat

Department of Physics, Faculty of Science and Mathematics, University of Zagreb, Yugoslavia

K. Ilakovac

Department of Physics, Faculty of Science and Mathematics, and Institute "R. Bošković," Zagreb, Yugoslavia
(Received 27 August 1984)

A pair of germanium detectors and a three-parameter analyzer were applied in an experimental study of the creation and of the decay of atomic states with a double K-shell vacancy, created in the decay of ^{109}Cd. Assuming a variable intensity ratio of the $K\alpha_1$ and $K\alpha_2$ hypersatellite lines, their shift with respect to the diagram lines, $\Delta^h_{K\alpha}=546\pm20$ eV, and the shift of the $K\alpha$ satellite lines with an initial L-shell vacancy, $\Delta^s_{K\alpha}(L^{-1})=54\pm6$ eV, were obtained. The former result is in agreement with the previous experimental result of van Eijk *et al.* and with the theoretical result of Chen *et al.*, but the latter result is significantly lower than the theoretical value of 73 eV. For the $I(K\alpha_1{}^h)/I(K\alpha^h)$ intensity ratio, a value of 0.54 ± 0.11 was obtained. From the numbers of counts in the hypersatellite-satellite peaks the intensity ratios of the hypersatellite lines $I(K\beta_1{}^h)/I(K\alpha^h)=0.195\pm0.016$, and $I(K\beta_2{}^h)/I(K\alpha^h)=0.055\pm0.008$ were obtained. The former value seems to be larger than the theoretical value 0.168, while the latter value is significantly larger than the theoretical value 0.029. Also the $I(K\beta_1{}^s)/I(K\alpha^s)$ and $I(K\beta_2{}^s)/I(K\alpha^s)$ intensity ratios of the satellite lines for the L-, M-, and N-shell initial spectator vacancies were derived. Within the errors the results are in agreement with the corresponding values for the diagram lines. The probability of creation of double K-shell vacancies per ^{109}Cd decay was determined to be $(6.07\pm1.12)\times10^{-5}$, in accord with the result $(6.25\pm0.54)\times10^{-5}$ of van Eijk *et al.*

I. INTRODUCTION

Due to the complexity of states and interactions, the studies of formation and of decay of atoms with a double vacancy in the K shell ("K^{-2} states") are very difficult and still require refinements. Experimental investigations are rather limited due to the very small probability of occurrence of these states. Among the various modes of creation of multiple vacancies in medium-heavy and heavy atoms, two nuclear decay processes warrant special attention: the internal-conversion (IC) and the electron-capture (EC) decay. We limit our considerations to transitions when sufficient energy is available for the removal of both electrons from the K shell. Then the removal of one electron from the K shell is most probable and K^{-1} states are created with high probability. Relative probabilities of creation of an additional vacancy, yielding, e.g., K^{-2}, $K^{-1}L^{-1}$, etc., states, are very low, while the creation of states with three or more initial vacancies is considered extremely rare. Therefore, when a K^{-2} state is created in an IC or EC decay it may be considered a very pure K^{-2} state. This is important to note in view of the high complexity of that state and of the states that follow in its decay.

Several mechanisms are considered to cause the ejection of the other K electron:[1] the shaking processes[2,3] [shake-up (SU) and shake-off (SO) processes], direct collision (DC) of the two electrons,[2] internal conversion in the internal Compton effect[4] (ICICE), internal conversion in the internal bremsstrahlung[5] (ICIB), and double internal conversion[6] (DIC). The experimental results indicate the

shaking processes to be dominant, but new measurements are required to clarify the situation. The large probabilities obtained from the simple theoretical expressions for ICICE (Ref. 4) are ruled out by experimental results,[7,8] but refined calculations of the process may show it to be important.

The properties and decay of the K^{-2} states have also been extensively studied. Since the original investigation of Briand *et al.*,[9] which has shown the existence of the new hypersatellite lines in x-ray spectra, and also yielded the energy shifts of hypersatellite lines in gallium, many investigations were performed.[7,8,10]

The decay of K^{-2} states seems to proceed predominantly via two independent transitions of electrons from higher shells, yielding a coincident pair of K x rays: a hypersatellite x ray (transition with a K-shell spectator vacancy) and a satellite x ray (transitions with an L-, M-, or N-shell spectator vacancy). A double-electron transition yielding a single-photon emission has also been observed,[11] but the relative probability is very low.

$^{109}_{48}$Cd is a very good "generator" of K^{-2} states. The decay scheme is shown in Fig. 1.[12] In the EC decay 81.5% is K capture. The probability of formation of K^{-2} states per K-electron capture was determined[8] at $P_{KK}(\text{EC})=(1.02\pm0.36)\times10^{-5}$. The electron-capture decay proceeds 100% directly to the 39.8-s—half-life metastable state of $^{109}_{47}$Ag. Because of the long half-life of the state, coincidences of radiations from the EC decay and the following decay of the metastable state are negligible. The metastable state decays by K conversion in 41.7% decays. The probability of creation of K^{-2} states per K
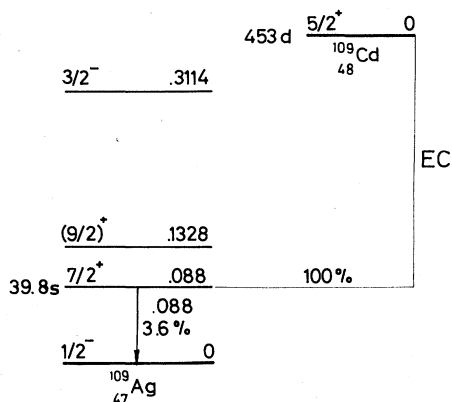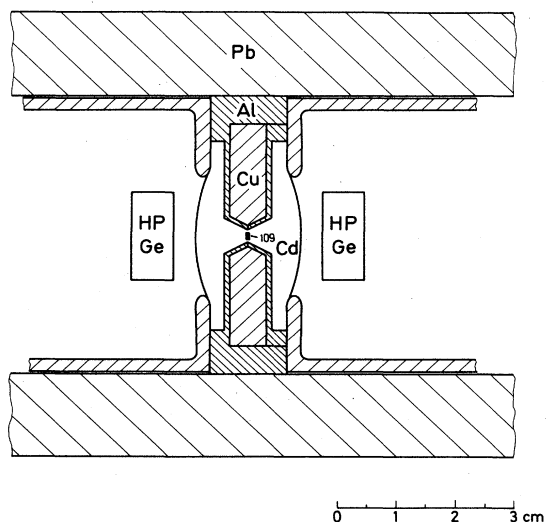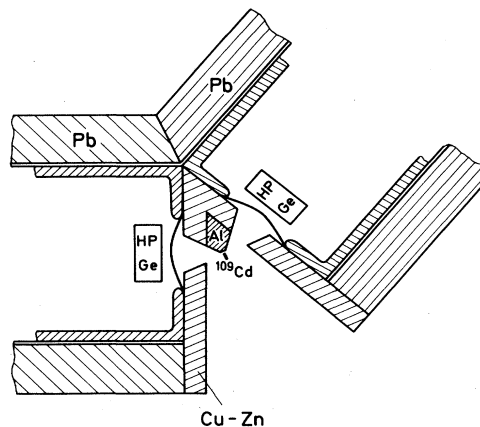
FIG. 1. Decay scheme of ^{109}Cd.

FIG. 3. Experimental arrangement in the 130° geometry.

internal conversion in this transition is[8] $P_{KK}(\text{IC})$ $=(13.0\pm1.1)\times10^{-5}$.

In this paper, in addition to a remeasurement of the probability of creation of K^{-2} states in the decay of ^{109}Cd and of the $K\alpha$ hypersatellite shift, we present new results: the $K\alpha$ satellite shift for an L-shell spectator vacancy, the relative intensities of $K\alpha$ and $K\beta$ hypersatellite lines, and some relative intensities of $K\alpha$ and $K\beta$ satellite lines.

II. MEASUREMENTS

Three series of measurements were made of 1553, 1172, and 1669 h duration. In the first and second series, 180° geometry was used (Fig. 2), and in the third series the angle between the source-to-detector centerlines was 130° (Fig. 3). In all measurements the sources were prepared by dripping a small amount of radioactive CdCl$_2$ in a 0.5N HCl solution (supplied by New England Nuclear, Boston) onto a small precut piece of pure cellulose paper 0.1-mm thick, followed by drying and mounting between two 0.6-mm-thick sheets of polyethylene. In the first series of measurements the diameter of the source was 1.6

mm, its initial strength was 0.84 kBq (1 Bq$=1$ s^{-1}), and the hole in the shield had a diameter of 2.0 mm. In the second series of measurements the diameter of the source was 0.5 mm, its initial strength was 1.15 kBq, and the hole in the shield had a diameter of 1.0 mm. In the third series of measurements the shielding between the detectors was arranged in such a way that direct scattering of photons from one detector into the other was prevented. The initial strength of the source was 2.43 kBq.

Two HP (high purity) germanium detectors (supplied by ORTEC, Oak Ridge) of nominal sensitive volumes 200 mm^2 by 7-mm thick were used as photon detectors. At 5.9 keV, their resolution was 210 and 230 eV, respectively. The outputs from the detectors were connected to a fast-slow coincidence system and a three-parameter pulse-height analyzer system (Fig. 4). For each coincidence event ($2\tau\approx250$ ns) the time difference (time channel, k_0) and the amplitudes of pulses from the detectors (energy channels, k_1 and k_2) were recorded. The data were analyzed off line in a UNIVAC 1110 computer.

A single measurement in the first and second series lasted for about four days and in the third series for about eight days. The apparatus was regularly tested before and after each measurement. Particular care was taken to assure the linear response of k_1 and k_2 channels with energy. Regular checks were made by connecting the output from a precision mercury pulse generator to the test inputs of both detectors. The differential linearity of the analog-to-digital converters (ADC's) was checked by means of a ramp pulser. The time scale was calibrated by inserting a 7-m-long coaxial cable either in the start or in
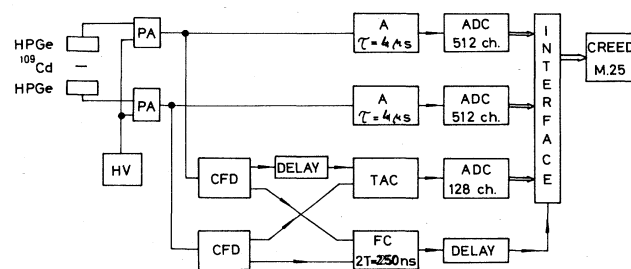

FIG. 2. Experimental arrangement in the 180° geometry.

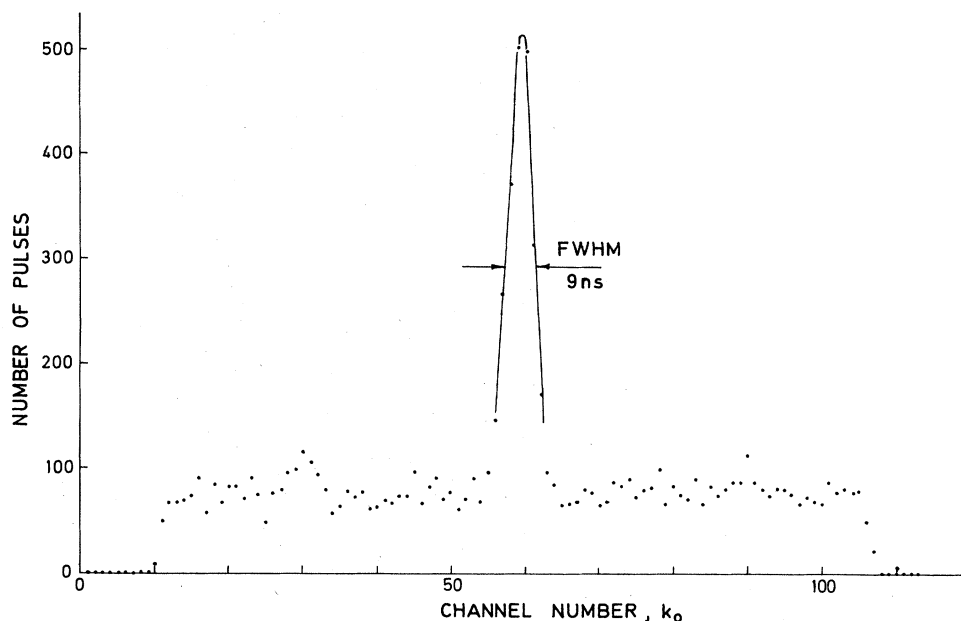FIG. 4. Block scheme of the electronic apparatus.

FIG. 5. Time spectrum in the region of hypersatellite-satellite peaks (k_1=400—512 and k_2=400—512) obtained from the data of the third series of measurements.

the stop line of the time-to-amplitude converter. The gain was 2.64 ns/channel. As an example, the time spectrum of the hypersatellite-satellite region (k_1=400—512 and k_2=400—512) of the third series of measurements is shown in Fig. 5. Full width at half maximum (FWHM) of the peak was 9 ns.

III. ANALYSIS OF DATA

The recorded data of the first series of measurements have shown a scatter in the positions of Ag $K\alpha_1$ peaks by almost two channels. They were divided into two records. Two further records were made from the data of the second and third series of measurements. The four records of data were independently analyzed.

Several routines were applied in the analysis of the data. Essential features were the selection of a k_1-k_2 region of interest, analysis of the time spectrum for the k_1-k_2 region, selection of an appropriate interval of time channels, preparation of the k_1-k_2 table of numbers of counts for the selected time interval, and fitting of the data in the table by an appropriate two-dimensional function, which was assumed to be a superposition of two-dimensional Gaussian functions integrated within channel limits, plus a constant (background). The size and the limits of the two-dimensional regions were chosen so that the contributions from the peaks outside the region could be neglected.

Time spectra were fitted by a constant (one parameter) plus a Gaussian function integrated within the channel limits (three parameters). The position of the maximum (k_0^{max}) and the standard deviation (σ_t) were used to determine the k_0 region for the analysis of coincident events (from $k_0^{max}-2\sigma_t$ to $k_0^{max}+2\sigma_t$) and the k_0 region for the analysis of accidental coincidences (below $k_0^{max}-4\sigma_t$ and above $k_0^{max}+4\sigma_t$). The limits of the k_0 regions were

rounded off to the closest integer values.

Accurate determination of energy scales for each of the four records was necessary for reliable analysis of contributions of the partially overlapped peaks in four regions of hypersatellite-satellite coincidences. The calibrations of channel numbers k_1 and k_2 versus energy were made by determining the positions of the peak maxima k_1^{max} and k_2^{max} of peaks in the k_1-k_2 field that were due to the known lines. Positions of Ge $K\alpha_1$ and Ag $K\alpha_1$ lines were basic, and positions at other lines were used for checks of linearity and to determine the accuracy of calibrations. The position of the peaks was determined from the data of the complete record. In this way it was assured that possible shifts would not impair the energy calibrations.

In the k_1-k_2 field several strong (Ag $Ka)_{Kb\ esc}$—Ge Kb peaks (a and b stand for α_1, α_2, $\beta_{1'}$, or $\beta_{2'}$), corresponding to the incomplete absorption of a Ka x ray incident upon one detector (due to the escape of a Ge Kb x ray), followed by the total absorption of the Ge Kb x ray in the other detector, were recorded. The four partially overlapped peaks due to the true coincidences of (Ag $K\alpha_1)_{K\alpha_1\ esc}$—Ge $K\alpha_1$, (Ag $K\alpha_1)_{K\alpha_2\ esc}$—Ge $K\alpha_2$, (Ag $K\alpha_2)_{K\alpha_1\ esc}$—Ge $K\alpha_1$, and (Ag $K\alpha_2)_{K\alpha_2\ esc}$—Ge $K\alpha_2$ x-ray pairs were fitted by four two-dimensional Gaussian functions of equal widths (for k_1 and k_2 coordinates separately). The known energies of the Ag $K\alpha$ and Ge $K\alpha$ x rays and relative intensities of the $K\alpha_1$ and $K\alpha_2$ lines were used,[12] while the variable parameters were the coordinates, the widths, and the amplitude of the (Ag $K\alpha_1)_{K\alpha_1\ esc}$—Ge $K\alpha_1$ peak and a uniform background.

The (Ag $K\alpha)_{K\alpha\ esc}$—Ge $K\alpha$ peaks were very weak in the measurements at 130°. Since no adjustments were made between the second and the third series, the energy zero points were assumed to be the same, and small

changes of the gain were taken into account by determining the positions of the second basic energy points. The second basic energy points, the coordinates k_1^{max} and k_2^{max} of the Ag $K\alpha_1$ diagram line, were determined in two ways. In the first approach four partially overlapped peaks due to accidental coincidences of Ag $K\alpha_1$–Ag $K\alpha_1$, Ag $K\alpha_1$–Ag $K\alpha_2$, Ag $K\alpha_2$–Ag $K\alpha_1$, and Ag $K\alpha_2$–Ag $K\alpha_2$ x-ray pairs were fitted by four two-dimensional Gaussian functions plus a uniform background. The variable parameters were the amplitude and the coordinates of the Ag $K\alpha_1$–Ag $K\alpha_1$ peak and the widths (separately for k_1 and k_2 dimensions) of the peaks, while the position and amplitudes of the three other peaks were calculated from the energy differences of α_1 and α_2 lines and from the intensity ratios of the diagram lines.[12] The widths obtained in this calculation were used in all further analyses. In the second approach the in-coincidence data were used to determine the coordinates of the Ag $K\alpha_1$–Ag $K\alpha_1$ peak as will be explained below. It may be noted that the very close agreement of the results for the energies per k_1 and k_2 channel (largest difference was about 0.15%) indicates an independence of the pulse-height analysis of the system on whether an in-coincidence or an out-of-coincidence event is recorded.

From the data in the region of hypersatellite-satellite peaks four k_1-k_2 tables of numbers of counts were prepared from each record. The tables contained the α-α group of peaks (Fig. 6), the α-β group of peaks (Fig. 7), the β-α group of peaks (the same as in Fig. 7 but with the k_1 and k_2 axes interchanged), and the β-β group of peaks (Fig. 8).

The data in the α-α regions were analyzed in two steps. In the first step nonlinear least-squares fits were applied because the positions of the peaks were assumed variable. The Poisson-statistics weights were applied. It is well known[13] that the fitting of a peak, with numbers of counts distributed according to the Poisson statistics, yields the total number of counts low by approximately the value of χ^2. A simple correction (adding of χ^2) can be applied if an isolated peak is analyzed. In the analyses of regions of hypersatellite-satellite peaks many peaks were involved with relatively low total numbers of counts and with considerable overlaps. The first steps were therefore aimed at the determination of the positions of the peaks and the second steps at the determination of the amplitudes of the peaks.

The data in the α-α regions were fitted by 20 two-dimensional Gaussian functions plus a constant background. (In the following, the diagram, satellite, and hypersatellite x rays will be denoted by superscripts d, s, and h, respectively.) The 20 functions represented five fourfold peaks: the peaks due to accidental coincidences of Ag $K\alpha^d$ x rays (D-D group in Fig. 6), the peaks due to true coincidences of Ag $K\alpha^h$ and Ag $K\alpha^s$ x rays (two H-S groups), and the peaks due to true coincidences of Ag $K\alpha^d$ and Cd $K\alpha^d$ x rays (two fourfold peaks, not indicated in Fig. 6).

In the first approach the energy scales were assumed known, so the positions of all peaks of known energy were fixed (Ag $K\alpha_1^d$—22.163 keV, Ag $K\alpha_2^d$—21.990 keV, Cd $K\alpha_1^d$—23.174 keV, and Cd $K\alpha_2^d$—22.984 keV). Fixed
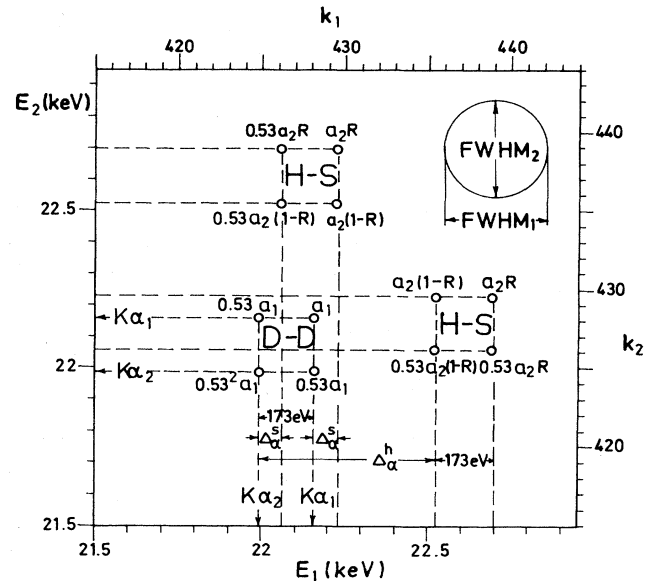

FIG. 6. α-α group of peaks. k_1 and k_2 are the channel numbers and E_1 and E_2 are the corresponding energies of photons. The positions of the $K\alpha_1$ and $K\alpha_2$ diagram lines are indicated by arrows. The group of four circles denoted by D-D shows the positions of the peaks due to accidental coincidences of ordinary $K\alpha$ x rays of silver, and the two groups of four circles each denoted by H-S show the positions of the peaks due to true coincidences of $K\alpha^h$ and $K\alpha^s$ x rays of silver. Two groups of four peaks each, due to true coincidences of Ag $K\alpha^d$ and Cd $K\alpha^d$ x rays, are not shown in the diagram. The amplitude of the $K\alpha_1^d$-$K\alpha_1^d$ peak is denoted by a_1 and the sum amplitudes of the $K\alpha_1^h$-$K\alpha_1^s$ and $K\alpha_2^h$-$K\alpha_1^s$ peaks by a_2. The $I(K\alpha_1^h)/[I(K\alpha_1^h)+I(K\alpha_2^h)]$ intensity ratio is denoted by R, and the hypersatellite and satellite shifts are denoted by $\Delta_{K\alpha}^h$ and $\Delta_{K\alpha}^s$, respectively.
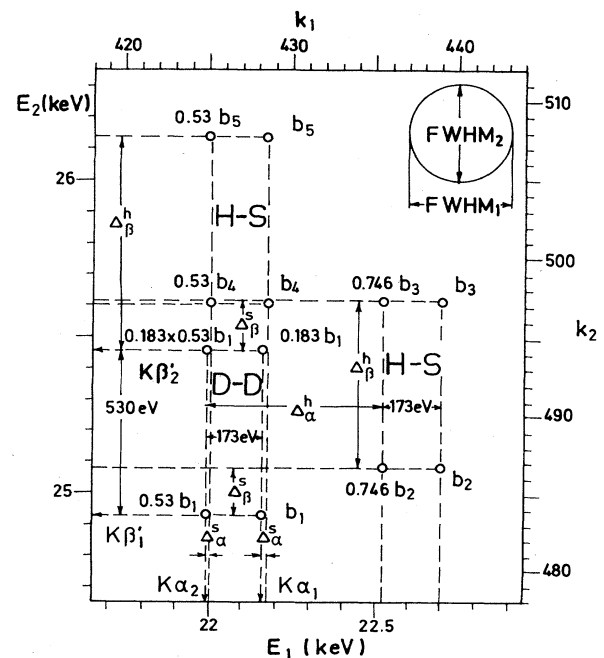

FIG. 7. α-β group of peaks. All symbols have the same or analogous meaning as in Fig. 6.

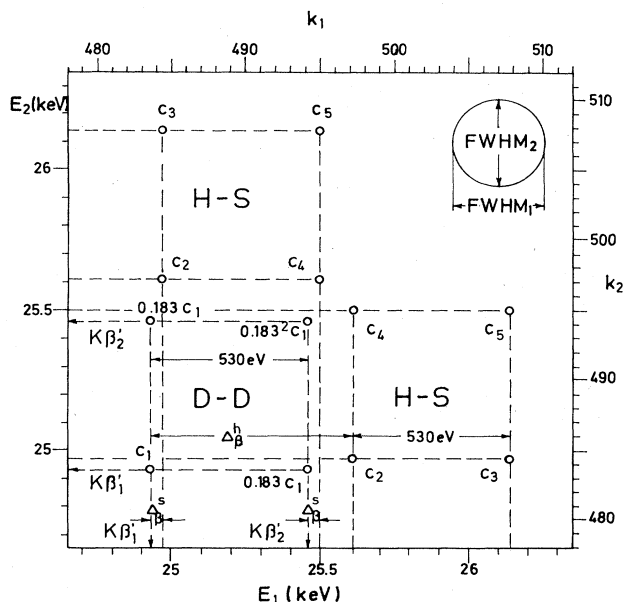FIG. 8. β-β group of peaks. All symbols have the same or analogous meaning as in Fig. 6.

values were also assumed for the widths of Gaussian functions, for the separation of Ag $K\alpha_1^s$ and Ag $K\alpha_2^s$, and Ag $K\alpha_1^h$ and Ag $K\alpha_2^h$ lines (both were assumed equal to the separation of Ag $K\alpha_1^d$ and Ag $K\alpha_2^d$ lines, 173 eV, because the calculated shifts[14] of the $K\alpha_1^h$ and $K\alpha_2^h$ are almost equal), and for the ratios of amplitudes of the Ag $K\alpha_2^d$ to Ag $K\alpha_1^d$ and Ag $K\alpha_2^s$ to Ag $K\alpha_1^s$ lines (these ratios were assumed equal). It should be noted that in the final calculations of errors the "fixed" parameters were changed, one by one, to the values plus and minus one standard deviation and the variations of the variable parameters of the fit were taken into account in the calculation of errors.

In the first step the variable parameters were the amplitude of the Ag $K\alpha_1^d$–Ag $K\alpha_1^d$ peak due to accidental coincidences (a_1), the amplitude of the Ag $K\alpha_{1,2}^h$–Ag $K\alpha_1^s$ peaks (a_2), the ratio of the amplitude of the Ag $K\alpha_1^h$ peak to the sum of the amplitudes of the Ag $K\alpha_1^h$ and Ag $K\alpha_2^h$ peaks (R), the satellite shift (Δ_α^s), the hypersatellite shift (Δ_α^h), the amplitude of the Ag $K\alpha_1$–Cd $K\alpha_1$ peaks (a_4), and a uniform background (Fig. 6). In the fit the values of all seven parameters were varied until the minimum of X^2 was reached. The values and errors obtained for $\Delta_{K\alpha}^s$, $\Delta_{K\alpha}^h$, and R were taken as final.

The error of the Ag $K\alpha$ hypersatellite shift ($\Delta_{K\alpha}^h$) was found to be relatively large due to the variability of the parameter R. Therefore, the fitting procedure was repeated assuming the value[14] $R = 0.573$. That assumption reduced considerably the error of the hypersatellite shift, its value did not change significantly, and the effect on other parameters was negligible.

In the second step the values of $\Delta_{K\alpha}^s$, $\Delta_{K\alpha}^h$, and R were fixed at the values obtained in the first step, and a linear least-squares fit to the data in the α-α region was made. 5×5 point smoothing with binomial coefficients was made, and the variances of the peaks were increased by

one.[13] In this way the amplitudes of the peaks were determined with a much smaller systematic error.

In the second approach in the analyses of the α-α regions one basic energy point was assumed, the Ge $K\alpha_1$ line (the k_1 and k_2 coordinates of the line were assumed to be the same as in the first approach). In fitting the incoincidence data in α-α regions, in addition to the seven variable parameters used in the first approach, two additional parameters were assumed variable, the energies per k_1 and per k_2 channel (ΔE_1 and ΔE_2, respectively). As was stated above, almost identical results were obtained for the energy scales and for the hypersatellite and satellite shifts, as in the first approach.

The second step of the second approach, the calculation of the amplitudes of the peaks, was also made by a different method. Since the energy scale and hypersatellite and satellite shifts were determined, coordinates of all peaks were known. The function of the fit was again represented by 20 two-dimensional Gaussian functions plus a uniform background. The background, however, was not assumed to be a variable parameter, but equal to the average value of the numbers of counts in parts of the analyzed α-α region that are distant from the peaks. In addition to the three variable amplitudes (a_1, $a_2' = a_2 R$, and a_4) also the amplitude of the Ag $K\alpha_2^h$–Ag $K\alpha_1^s$ peak [$a_3 = (1 - R)a_2$] was introduced as a variable parameter. Instead of smoothing of the data, equal weights were assumed for all numbers of counts.

In the analyses of α-β, β-α, and β-β regions the numbers of counts were not sufficient to allow the determination of either hypersatellite or satellite shifts. The Ag $K\alpha$ and Ag $K\beta_1'$ hypersatellite shifts were assumed equal to the values from Ref. 14, and the Ag $K\beta_2'$ hypersatellite shift was assumed equal to the Ag $K\beta_1'$ hypersatellite shift. The satellite shifts were derived from Ref. 14 and from the results of Wolter, Burch, and Richard presented in Ref. 15 except for the shifts of the $K\beta_1'^s$ and $K\beta_2'^s$ lines emitted with an M- or an N-shell spectator vacancy, which were estimated at 40 eV. The ±10-eV changes of the satellite shifts were found to have a negligible effect on the variable parameters of the fit. Linear least-squares fits (analogous to the second-step analyses of the α-α regions) were made to determine the amplitudes of the peaks. The data in the α-β regions, and similarly in β-α regions, were represented by 12 peaks indicated in Fig. 7 and by six additional peaks (true coincidences of Ag $K\alpha_{1,2}^d$–Cd $K\beta_1^d$ and Ag $K\beta_{1,2}^d$–Cd $K\alpha_{1,2}^d$ x-ray pairs), i.e., 18 two-dimensional Gaussian functions, plus uniform backgrounds. The variable parameters, the amplitudes $b_1, b_2, \ldots, b_5$, and the fixed parameters are shown in Fig. 7. The data in the β-β regions were represented by 12 peaks indicated in Fig. 8 and by four additional peaks (due to true coincidences of Ag $K\beta_{1,2}^d$–Cd $K\beta_1^d$ x-ray pairs), i.e., 16 peaks, plus a uniform background. The variable parameters, the amplitudes $c_1, c_2, \ldots, c_5$, and the fixed parameters are shown in Fig. 8. The two approaches applied in the analyses of α-α regions were extended in the analyses of α-β, β-α, and β-β regions. In the first approach a 5×5 point smoothing with binomial coefficients was applied to the data, the variances of the peaks were enlarged by one, and the uniform background

was assumed to be a variable parameter, while in the second approach equal weights were assumed for all numbers of counts, and the background was taken equal to the average value of numbers of counts in parts of the analyzed regions that are far from the peaks.

The results of the analyses by the first and by the second approaches are generally in good agreement. For example, the weighted average of the results for the hypersatellite shift [variable $I(K\alpha_1^h)/I(K\alpha_2^h)$ ratio] are 545 ± 30 and 547 ± 20 eV, for the satellite shift are 55.6 ± 5.6 and 50.7 ± 7.1 eV, and for the $I(K\alpha_1^h)/[I(K\alpha_1^h)+I(K\alpha_2^h)]$ ratio are 0.55 ± 0.15 and 0.53 ± 0.11. From the amplitudes of the two-dimensional peaks in the α-α, α-β, β-α, and β-β regions the numbers of counts shown in Fig. 9 were calculated. Since the contributions of the $K\alpha_1^d$ and $K\alpha_2^d$, $K\alpha_1^s$ and $K\alpha_2^s$, and $K\alpha_1^h$ and

FIG. 9. The numbers of counts in the peaks in the α-α, α-β, β-α, and β-β regions. The peaks due to true coincidences are indicated by full circles and the peaks due to accidental coincidences by dashed circles. The $K\alpha_1$ and $K\alpha_2$ lines are not separately shown. The circles denoted by A, B, and C represent the peaks due to the coincident detection of $K\alpha^h$ x rays in detector No. 1 and of $K\alpha^s$, $K\beta_1^s$, or $K\beta_2^s$ x rays in detector No. 2, while the circles indicated by A', B', and C' represent the same peaks but with the roles of the detectors interchanged. Similarly, D, E, and F (and D', E', and F') represent the peaks due to the coincident detection of $K\beta_1^h$ x rays and $K\alpha^s$, $K\beta_1^s$, or $K\beta_2^s$ x rays, and G, H, and I (and G', H', and I') represent the peaks due to the coincident detection of $K\beta_2^h$ x rays and $K\alpha^s$, $K\beta_1^s$, or $K\beta_2^s$ x rays. The four numbers in the circles show the numbers of counts in the peaks obtained in the analyses of the four records of data. For the symmetrical peaks in the α-α and β-β regions the sums of numbers of counts are given. The satellite transitions that follow the $K\alpha^h$, $K\beta_1^h$, and $K\beta_2^h$ transitions lay along the lines indicated by the L-, M-, and N-shell spectator vacancies.

$K\alpha_2^h$ lines were not well separated, the numbers of counts are given jointly for these lines, and so are the results for the symmetrical peaks in α-α and β-β groups because they were analyzed assuming equal amplitudes. In Fig. 9 the numbers of counts in the Ag $K\alpha^d$—Cd $K\alpha_1^d$ groups of peaks are not shown. Total numbers of counts in both of these groups were 38, 43, 81, and 61 counts for the four records, respectively.

IV. RESULTS AND DISCUSSION

The result obtained for the intensity ratio of the $K\alpha_1^h$ and the sum of intensities of $K\alpha_1^h$ and $K\alpha_2^h$ lines,

$$R = I(K\alpha_1^h)/[I(K\alpha_1^h)+I(K\alpha_2^h)] = 0.54\pm0.11 ,$$

is not very accurate because the energy difference of the two x rays, 173 eV, is smaller than the resolution of the detectors used in the measurements. It agrees both with the result for the diagram lines, 0.654,[12] and with the value 0.573 derived from the theoretical result $I(K\alpha_1^h)/I(K\alpha_2^h)=1.34$ of Chen et al.[14]

The result for the hypersatellite shift of the $K\alpha^h$ lines, obtained when the ratio R was assumed variable (it should be noted that for silver this ratio has not previously been experimentally determined), is

$$\Delta_{K\alpha}^h = 546\pm20 \text{ eV} .$$

This result agrees well with the theoretical result of Chen et al.[14] (535.0 and 534.3 eV for the $K\alpha_1^h$ and $K\alpha_2^h$ lines, respectively). For comparison with the earlier result of van Eijk et al.,[8] $\Delta_{K\alpha}^h=532\pm6$ eV, the nonlinear least-squares fits were also made with a fixed value $R=0.573$. The result is $\Delta_{K\alpha}^h=539\pm7$ eV.

The result for the shift of the $K\alpha$ satellite line with an "initial" L-shell spectator vacancy (with respect to the $K\alpha$ diagram line),

$$\Delta_{K\alpha}^s(\text{initial } L\text{-shell vacancy})=54\pm6 \text{ eV} ,$$

is significantly lower than the theoretical result $\Delta_{K\alpha}^s(L^{-1})=73$ eV of Wolter, Burch, and Richard and the result 67 eV of an approximate calculation of Burch et al.[15] The L-level and K-level widths (for ordinary x-ray transitions—no spectator vacancies) are comparable, 2 and 5.6 eV, respectively.[16] Therefore, one can expect that a $K^{-1}L^{-1}$ state, formed from a K^{-2} state after the emission of a $K\alpha^h$ x ray, can also decay by first emitting an L^h (K-shell spectator vacancy) x ray, followed by a $K\alpha^s$ (M- or N-shell spectator vacancy) x ray. Therefore, in the present experiment some mean value of the $K\alpha^s(L^{-1})$, $K\alpha^s(M^{-1})$, and $K\alpha^s(N^{-1})$ shifts was measured which is expected to have a lower value than the $K\alpha^s(L^{-1})$ shift.

The intensity ratios of the K x rays were calculated from the results on numbers of counts in the peaks in the analyzed α-α, α-β, β-α, and β-β regions. The relative detection efficiency of the detectors was calculated from the expression for the probability of escape of characteristic radiation from germanium detectors.[17] For photons of energies of about 22.5, 25.5, and 26.1 keV the values 0.932, 0.947, and 0.950 were obtained, respectively.

The values of the $[I(K\beta_1^d)+I(\beta_2^d)]/I(K\alpha^d)$ intensity ratios calculated from the numbers of counts in the peaks
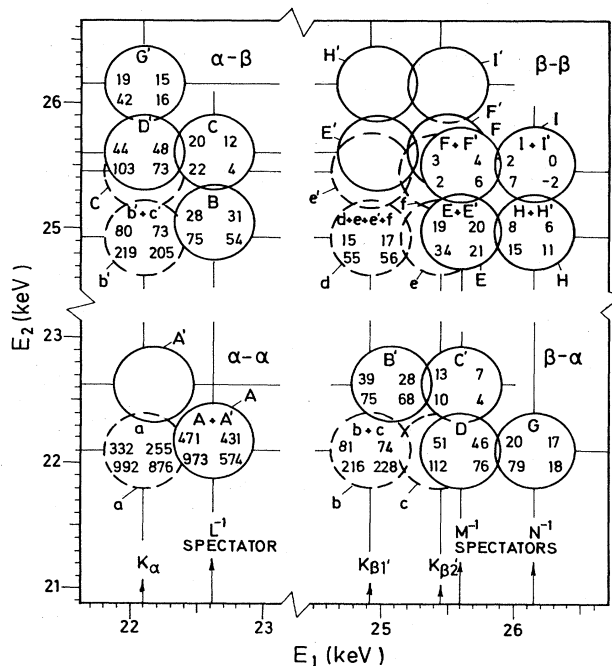
due to accidental coincidences of ordinary K x rays (lower-case letters in Fig. 9) are higher than the accepted value, 0.211, between about 5% and 30%. Mean deviation is $15\pm8\%$. Although this result may roughly be considered as an agreement, taking into account the possibility of some instrumental cause of the observed deviations (e.g., variation of the coincidence efficiency with energy, or absorption), the results on intensity ratios of hypersatellite and satellite transitions were corrected for the factors calculated as the ratio of the measured $[I(K\beta_1{}^d)+I(K\beta_2{}^d)]/I(K\alpha^d)$ intensity ratio and the value 0.211, separately for each record.

The $I(K\beta_1{}^h)/I(K\alpha^h)$ and $I(K\beta_2{}^h)/I(K\alpha^h)$ intensity ratios were calculated in two ways, from the data in the peaks that correspond to the hypersatellite transitions in the k_1 coordinate and from the data in the peaks that correspond to the hypersatellite transitions in the k_2 coordinate. Thus, the data denoted by A, B, and C; D, E, and F; and G, H, and I were first used to calculate the intensities of $K\alpha^h$, $K\beta_1{}^h$, and $K\beta_2{}^h$ lines, respectively. Then the data denoted by A', B', and C'; D', E', and F'; and G', H', and I' were used to calculate the intensities of the same lines. All numbers of counts that were calculated by the least-squares fits assuming equal amplitudes of the pairs of symmetrical peaks (A-A', E-E', F-F', H-H', and I-I') were given the values equal to half of the sum, i.e., $A=A'=\frac{1}{2}(A+A')$, etc. From the eight values for the $I(K\beta_1{}^h)/I(K\alpha^h)$ and $I(K\beta_2{}^h)/I(K\alpha^h)$ intensity ratios the weighted averages shown in Table I were calculated.

The emission of a $K\alpha^h$ x ray yields a $K^{-1}L^{-1}$ state and the following satellite x-ray transitions have initially an L-shell spectator vacancy. Hence, the numbers of counts in the hypersatellite-satellite peaks corresponding to the coincident detection of a $K\alpha^h$ x ray and $K\alpha^s$, $K\beta_1{}^s$, and $K\beta_2{}^s$ x rays in the other detector can be used for the calculation of the $I(K\beta_1{}^s)/I(K\alpha^s)$ and $I(K\beta_2{}^s)/I(K\alpha^s)$ intensity ratios with an initial L-shell spectator vacancy. These ratios were also calculated in two ways, from the numbers of counts in the peaks A, B, and C and from the numbers of counts in the peaks A', B', and C'. Similarly, the $I(K\beta_1^s{}_{'})/I(K\alpha^s)$ and $I(K\beta_2{}^s)/I(K\alpha^s)$ intensity ratios with the initial M-shell spectator vacancy were calculated from the numbers of counts in the peaks D, E, and F and D', E', and F', and the $I(K\beta_1{}^s)/I(K\alpha^s)$ and $I(K\beta_2{}^s)/I(K\alpha^s)$ intensity ratios with the initial N-shell spectator vacancy were calculated from the numbers of counts in the peaks G, H, and I and G', H', and I'. In the calculations of these ratios the above-mentioned calculated efficiencies of the detectors were used, and the re-

sults were corrected for the deviation of the $[I(K\beta_1{}_{'}+I(K\beta_2{}_{'})]/I(K\alpha)$ intensity ratio from the value 0.211 for the diagram lines, separately for each record. From the eight values obtained for the $I(K\beta_1{}^s)/I(K\alpha^s)$ and $I(K\beta_2{}^s)/I(K\alpha^s)$ intensity ratios with initial L-, M-, and N-shell spectator vacancies the weighted averages shown in Table I were calculated.

The result for the $I(K\beta_1{}^h)/I(K\alpha^h)$ intensity ratio seems to indicate a larger value than the theoretical value of Chen et al.[14] and than the value of the corresponding ratio for the diagram lines. The result for the $I(K\beta_2{}^h)/I(K\alpha^h)$ intensity ratio is larger than the theoretical value[14] by more than three standard errors and larger than the corresponding ratio for the diagram lines by almost three standard errors. The results for the $I(K\beta_1{}^s)/I(K\alpha^s)$ intensity ratios seem to be a little smaller than the value of the corresponding ratio for the diagram lines, but, within experimental errors, may also be considered to be equal, as is usually assumed. The values for the $I(K\beta_2{}^s)/I(K\alpha^s)$ intensity ratios are not very accurate.

N_0 decays of ^{109}Cd atoms are accompanied by the emission of $N_0[p_K(\text{EC})+p_K(\text{IC})]\omega_K$ K x rays of silver, where $p_K(\text{EC})=0.815\pm0.002$ is the probability of K capture in EC decay of ^{109}Cd, $p_K(\text{IC})=0.417\pm0.002$ is the probability of K-electron internal conversion in ^{109}Ag, and $\omega_K=0.830$ is the K-shell fluorescence yield of silver atoms.[12] At the same time the total number of hypersatellite-satellite K x-ray pairs emitted from the source is equal to

$$N_0[p_K(\text{EC})P_{KK}(\text{EC})+p_K(\text{IC})P_{KK}(\text{IC})]\omega_K^h\omega_K^s ,$$

where $P_{KK}(\text{EC})$ and $P_{KK}(\text{IC})$ are the probabilities of creation of K^{-2} states per K capture in ^{109}Cd and per K internal conversion in ^{109m}Ag, respectively, and ω_K^h and ω_K^s are the fluorescence yields of hypersatellite and satellite transitions in silver atoms, respectively. Taking into account the geometry of the experimental arrangement, the probability of creation of a K^{-2} state per decay of a ^{109}Cd (and ^{109m}Ag) atom can be calculated from the relation

$$p_K(\text{EC})P_{KK}(\text{EC})+p_K(\text{IC})P_{KK}(\text{IC})$$

$$=[p_K(\text{EC})+p_K(\text{IC})]\frac{n_{\text{hs}}}{n_1}\frac{\omega_K}{\omega_K^h\omega_K^s}\frac{4\pi}{\Omega_2}\frac{\langle\epsilon_1\rangle}{\langle\epsilon_1\epsilon_2\epsilon_c\rangle} ,$$

where n_{hs} is the total number of counts in all

TABLE I. The $I(K\beta_1{}_{'})/[I(K\alpha_1)+I(K\alpha_2)]$ and $I(K\beta_2{}_{'})/[I(K\alpha_1)+I(K\alpha_2)]$ intensity ratios in silver atoms.

	Hypersatellite lines		Satellite lines			Diagram lines
Initial spectator vacancy	K^{-1}		L^{-1}	M^{-1}	N^{-1}	None
Intensity ratio	Theory	Experiment	Experiment	Experiment	Experiment	Ref. 12
$I(K\beta_1{}_{'})/[I(K\alpha_1)+I(K\alpha_2)]$	0.168	0.195 ± 0.016	0.152 ± 0.016	0.155 ± 0.020	0.19 ± 0.06	0.178
$I(K\beta_2{}_{'})/[I(K\alpha_1)+I(K\alpha_2)]$	0.0293	0.055 ± 0.008	0.034 ± 0.011	0.027 ± 0.013	0.02 ± 0.05	0.0327

hypersatellite-satellite peaks, n_1 is the total number of K x rays detected in detector 1, Ω_2 is the solid angle of detector 2, and $\langle \epsilon_1 \rangle$ and $\langle \epsilon_1 \epsilon_2 \epsilon_c \rangle$ are the overall x-ray-lines averaged efficiency of detector 1 and of the coincidence system, respectively, and

$$\langle \epsilon_1 \rangle = \sum_{\xi} W_{K\xi} \epsilon_1(K\xi) \Big/ \sum_{\xi} W_{K\xi} \, ,$$

where $\xi = \alpha$, $\beta_{1'}$, and $\beta_{2'}$, $W_{K\xi}$ is the relative intensity of the $K\xi$ x ray, and $\epsilon_1(K\xi)$ is the relative detection efficiency of detector 1 for $K\xi$ x rays, and

$$\langle \epsilon_1 \epsilon_2 \epsilon_c \rangle = \sum_{\xi_1} \sum_{\xi_2} W_{K\xi_1}^h W_{K\xi_2}^s [\epsilon_1^h(K\xi_1)\epsilon_2^s(K\xi_2) + \epsilon_1^s(K\xi_1)\epsilon_2^h(K\epsilon_2)] \epsilon_c(K\xi_1, K\xi_2) \Big/ \sum_{\xi_1} \sum_{\xi_2} W_{K\xi_1}^h W_{K\xi_2}^s \, ,$$

where $W_{K\xi}^h$ and $W_{K\xi}^s$ are the relative intensities of $K\xi^h$ and $K\xi^s$ x rays, $\epsilon_i^h(K\xi)$ and $\epsilon_i^s(K\xi)$ are the detection efficiencies of the detectors for the $K\xi^h$ and $K\xi^s$ x rays, and $\epsilon_c(\xi_1, \xi_2)$ is the efficiency of the coincidence for a pair of $K\xi_1^h - K\xi_2^s$ x rays.

From the results shown in Fig. 9 one obtains $n_{hs} = 737$, 665, 1520, and 925 counts, respectively, while the numbers of K x rays detected in full-energy peaks are 1.40×10^8, 1.27×10^8, 2.78×10^8, and 4.62×10^8 for the four records, respectively.

The average efficiencies were estimated at $\langle \epsilon_1 \rangle = 0.94$ and $\langle \epsilon_1 \epsilon_2 \epsilon_c \rangle = 2 \times 0.84$, and the solid angle of the detectors (very nearly equal for the first three records) was $4\pi \times 0.0615$, and for the fourth record $4\pi \times 0.034$. From the data the following probabilities of creation of K^{-2} states per ^{109}Cd decay were obtained: $(7.13 \pm 0.60) \times 10^{-5}$, $(7.06 \pm 0.73) \times 10^{-5}$, $(7.39 \pm 1.15) \times 10^{-5}$, and $(4.89 \pm 0.46) \times 10^{-5}$ for the four records, respectively. The mean value of the results,

$$[p_K(\text{EC})P_{KK}(\text{EC}) + p_K(\text{IC})P_{KK}(\text{IC})]$$
$$= (6.07 \pm 1.12) \times 10^{-5} \, ,$$

is in good agreement with the result of van Eijk et al., $(6.27 \pm 0.54) \times 10^{-5}$.

[1] T. Mukoyama, Y. Isozumi, T. Kitahara, and S. Shimizu, Phys. Rev. C **8**, 1308 (1973); M. S. Freedman, Annu. Rev. Nucl. Sci. **24**, 209 (1974); R. J. Walen and Ch. Briançon, in *Atomic Inner Shell Processes*, edited by B. Crasemann (Academic, New York, 1975); W. Bambynek, H. Behrens, M. H. Chen, B. Crasemann, M. L. Fitzpatrick, K. W. D. Ledingham, H. Genz, M. Mutterer, and R. L. Intemann, Rev. Mod. Phys. **49**, 77 (1977).

[2] E. L. Feinberg, J. Phys. (Moscow) **4**, 423 (1941); Yad. Fiz. **1**, 612 (1965) [Sov. J. Nucl. Phys. **1**, 438 (1965)].

[3] A. Migdal, J. Phys. (Moscow) **5**, 449 (1941); H. Primakoff and F. T. Porter, Phys. Rev. **89**, 930 (1953); T. A. Carlson, C. W. Nestor, Jr., and T. C. Tucker, *ibid.* **169**, 27 (1968); P. Stephas and B. Crasemann, Phys. Rev. C **3**, 2495 (1971); R. L. Intemann, Phys. Rev. **188**, 1963 (1969); A. J. Nord, Nucl. Phys. **A192**, 305 (1972); T. Mukoyama and S. Shimizu, Phys. Rev. C **11**, 1353 (1975); **13**, 377 (1976); A. Suzuki and J. Law, *ibid.* **25**, 2722 (1982).

[4] M. A. Listengarten, Vestn. Leningr. Univ. Ser. Mat. Fiz. Khim. **16**, 142 (1962).

[5] T. Mukoyama and Gábor Hock (private communication); K. Pisk, M. Krčmar, and B. A. Logan, Phys. Rev. C **27**, 1260 (1983).

[6] J. Eichler, Z. Phys. **160**, 333 (1960); D. P. Grechukhin, Yad. Fiz. **4**, 497 (1966) [Sov. J. Nucl. Phys. **4**, 354 (1967)].

[7] H. J. Nagy, G. Schupp, and R. R. Hurst, Phys. Rev. C **11**, 205 (1975).

[8] C. W. E. van Eijk, J. Wijnhorst, and M. A. Popelier, Phys. Rev. C **19**, 1047 (1979).

[9] J. P. Briand, P. Chevallier, M. Tavernier, and J. P. Rozet, Phys. Rev. Lett. **27**, 777 (1971).

[10] H. J. Nagy, G. Schupp, and R. R. Hurst, Phys. Rev. C **6**, 607 (1972); J. P. Desclaux, Ch. Briancon, J. P. Thibaud, and R. J.

Walen, Phys. Rev. Lett. **32**, 447 (1974); R. Javahery, C. W. E. van Eijk, H. van Krugten, and B. van Nooijen, Phys. Rev. A **10**, 1921 (1974); J. P. Briand, P. Chevallier, A. Johnson, J. P. Rozet, M. Tavernier, and A. Touati, Phys. Lett. **49A**, 51 (1974); K. Schreckenbach, H. G. Börner, and J. P. Desclaux, *ibid.* **63A**, 330 (1977); C. W. E. van Eijk, J. Wijnhorst, and M. A. Popelier, Phys. Rev. A **20**, 1749 (1979); **24**, 854 (1981); S. I. Salem, *ibid.* **21**, 858 (1980); J. P. Briand, P. Chevallier, A. Chetioui, J. P. Rozet, M. Tavernier, and A. Touati, *ibid.* **23**, 39 (1981); C. W. E. van Eijk, J. P. Wagenaar, F. Bergsma, and W. Lourens, *ibid.* **26**, 2749 (1982); Y. Isozumi, Ch. Briançon, and R. J. Walen, Phys. Rev. C **25**, 3078 (1982); H. J. Nagy and G. Schupp, *ibid.* **27**, 2887 (1983).

[11] Y. Isozumi, Phys. Rev. A **22**, 1948 (1980); W. Wölfli, Ch. Stoller, G. Bonani, M. Suter, and M. Stöckli, Phys. Rev. Lett. **35**, 656 (1975); Phys. Rev. A **15**, 990 (1977); Th. Hoogkamer, P. Woerlee, F. W. Saris, and M. Gavrila, J. Phys. B **9**, L145 (1976); I. V. Mitchell, W. N. Lennard, and D. Phillips, Phys. Rev. A **16**, 1723 (1977).

[12] C. M. Lederer and V. S. Shirley, *Table of Isotopes*, 7th ed. (Wiley-Interscience, New York, 1978).

[13] P. R. Bevington, *Data Reduction and Error Analysis for the Physical Sciences* (McGraw-Hill, New York, 1969).

[14] M. H. Chen, B. Crasemann, and H. Mark, Phys. Rev. A **25**, 391 (1982).

[15] D. Burch, L. Wilets, and W. E. Meyerhof, Phys. Rev. A **9**, 1007 (1974), and references therein.

[16] W. Bambynek, B. Crasemann, R. W. Fink, H.-U. Freund, H. Mark, C. D. Swift, R. E. Price, and P. Venugopala Rao, Rev. Mod. Phys. **44**, 716 (1972).

[17] M. P. Fioratti and S. R. Piermattei, Nucl. Instrum. Methods **96**, 605 (1971).